Poly-amide modified copper foam electrodes for enhanced electrochemical reduction of carbon dioxide

Sunyhik Ahn, Konstantin Klyukin, Russell Jon Wakeham, Jennifer Rudd, Aled R. Lewis, Shirin Alexander, Francesco Carla, Vitaly Alexandrov, and Enrico Andreoli

ACS Catal., **Just Accepted Manuscript** • DOI: 10.1021/acscatal.7b04347 • Publication Date (Web): 03 Apr 2018

Poly-Amide Modified Copper Foam Electrodes for Enhanced Electrochemical Reduction of Carbon Dioxide

Sunyhik Ahn,[†] Konstantin Klyukin,[‡] Russell J. Wakeham,[†] Jennifer A. Rudd,[†] Aled R. Lewis,[†] Shirin Alexander,[†] Francesco Carla,[¶] Vitaly Alexandrov,[‡] and Enrico Andreoli*,[†]

†*Energy Safety Research Institute, Swansea University, Bay Campus, Swansea, SA1 8EN, UK*

‡*Department of Chemical and Biomolecular Engineering, University of Nebraska-Lincoln, 207E Othmer Hall, Lincoln, Nebraska, USA*

¶*European Synchrotron Radiation Facility, CS 40220, 38043, Grenoble Cedex 9, France*

E-mail: e.andreoli@swansea.ac.uk

Abstract

A strategy to modulate the electrocatalytic activity of copper towards CO_2 reduction involving adsorption of acrylamide, acrylic acid and allylamine polymers is presented. Modification of electrodeposited copper foam with poly(acrylamide) leads to a significant enhancement in faradaic efficiency for ethylene from 13% (unmodified foam) to 26% at -0.96 V vs. RHE, whereas methane yield is unaffected. Effects from crystalline phase distribution and copper oxide phases are ruled out as the source of enhancement through XPS and in-situ XRD analysis. DFT calculations reveal that poly(acrylamide) adsorbs on the copper surface via the oxygen atom on the carbonyl groups, and enhances ethylene formation by i) charge donation to the copper surface that activates

CO for dimerization, ii) chemical stabilization of the CO dimer (a key intermediate for C_2 products) by hydrogen-bond interactions with the -NH_2 group, and iii) facilitating the adsorption of CO molecules near the polymer, increasing local surface coverage. Poly(acrylamide) with copper acts as a multi-point binding catalytic system where the interplay between activation and stabilization of intermediates results in enhanced selectivity toward ethylene formation. Modification with poly(acrylic acid) which has a similar structure to poly(acrylamide) also shows some enhancement in activity but is unstable, whereas poly(allylamine) completely suppresses CO_2 reduction in favor of the hydrogen evolution reaction.

Keywords

electrocatalysis, greenhouse gas, heterogeneous catalyst, modified electrodes, ethylene, DFT, blue moon

1 Introduction

With growing awareness on the accumulation of anthropogenic carbon dioxide in the atmosphere and the associated negative impact on the environment, CO_2 capture for storage and conversion into value-added products has become a topic of intense research.[1,2] Conversion of CO_2 into hydrocarbons and alcohols which effectively cyclize the carbon fuel economy is an attractive prospect given the tremendous infrastructure already in place for the transport, storage and utilization of these fuels. Ethylene in particular is an important industrial feedstock consumed at a megaton scale annually, of which nearly 100% is sourced by cracking non-renewable fossil fuels.

A range of transition metals exhibit electrocatalytic activity for CO_2 reduction.[3,4] However, the activity and selectivity of catalysis is highly dependent on the strength of interaction

between the reaction intermediates and the metal catalyst. In the case of CO_2 reduction, copper is considered to be nearly the ideal case with the right balance of reaction intermediate binding strength for stabilization of COOH*, CO* and CHO* species (leading to hydrocarbons), that is not so strong that the intermediates are inhibited from further reaction steps and release.[3,4] A fundamental problem with mediating multi-step electron transfer reactions on conventional heterogeneous catalysts lay with non-optimal 'scaling relations' that exist between reaction intermediates, which effectively reduces the number of independently tunable parameters for optimization of catalytic performance.[5,6]

Since Hori reported copper mediated aqueous CO_2 reduction in 1985,[3] the field has continued to grow with studies on copper oxide derived catalysts,[7–10] copper single crystals,[11,12] molecular copper complexes,[13,14] and copper nanostructures.[15–17] However, many of the copper catalysts reported exhibit lower activity for CO_2 reduction than Hori's copper foils, when compared in terms of geometric partial current for hydrocarbon formation (Fig. S1). Here, geometric partial current density (as opposed to electrochemically active surface area normalized partial current density) is chosen as the benchmarking quantifier for catalyst performance as it gives a practical feel for how the material will scale inside a physical electrolyzer set-up. There is a need to develop scale-able high-surface area catalysts for higher throughput hydrocarbon formation. Sen et al. investigated electrodeposited copper foams with a dull 'reddish' appearance, and found CO_2 was reduced into hydrocarbons with a faradaic yield of ca. 2% (at -1.7 V vs. Ag/AgCl).[18] The same group showed that this could be increased to 4% with the addition of clathrate hydrate to the electrolyte which improved the solubility of CO_2.[19] Dutta et al. investigated copper foams electrodeposited under similar conditions to Sen, but the foams were black in appearance and reduced CO_2 into hydrocarbons with 50% faradaic efficiency with ethane being the dominant product.[20] The authors attributed the difference in activity to oxide derived copper formed through a room-temperature surface oxidation step. More recently, Reller et al. reported copper foams

in KBr electrolyte reduced CO_2 into hydrocarbons with up to 57% faradaic efficiency with a current density of 170 $mAcm^{-2}$.[21] While the study is of fundamental interest, use of KBr electrolyte is practically undesirable as it leads to generation of toxic bromine gas on the anode and corrosion of copper.

Modification of copper with additives such as polyaniline,[22] poly(4-vinyl pyridine),[23] polysulfide,[24] and cyclams[25] has been reported to increase selectivity for formate production. Polypyrrole coated copper in methanol electrolyte led to an increase in faradaic efficiency for methane, but 20 bar pressure was required.[26] Xie et al., recently showed that drop-casting glycine on copper foil electrode led to the enhancement of the faradaic efficiency of methane from 16.1% to 32.1% and ethylene from 9.5% to 24% both at -1.9 V vs. Ag/AgCl.[27] The study rationalized this through DFT calculations which simulated a chemical stabilization effect of the CHO* intermediate by $-NH_3^+$ groups on surface bound amino acids. However, it is unclear why other amino acids tested which also contain the $-NH_3$ group show varying performance levels compared to the optimal case of glycine. Some of the above cited studies do not take ohmic drop effects into account, which makes direct comparison across different modification strategies difficult (see Fig. S2 for further discussion). This study expands the work on copper foams whose large surface area and ease of synthesis offers favorable scale-ability compared to other reported materials. We report for the first time, a convenient catalyst modification strategy based on coating metallic electro-catalysts with polymers which significantly enhances the efficiency for hydrocarbon formation. The initial basis for the use of polyamines with copper was that CO_2 is known to bind to amines to form carbamates.[28–30] It was hoped that the amine-CO_2 interaction would lower the activation energy required for CO_2 reduction. Tethering functional groups that affect the catalytic reaction kinetics offer an additional independently tunable parameter for the optimization and design of more efficient catalysts for CO_2 reduction.

2 Experimental

2.1 Electrode preparation

3 mm diameter copper rod (99.99%, Goodfellow, UK) was cut into cylindrical pieces and embedded into a polycarbonate body with Araldite epoxy (Huntsman Advanced Materials, Switzerland). The electrode was mechanically polished with 0.3 μm alumina slurry followed by rinsing and ultra-sonication in deionized water for 1 minute. Copper foam was electrodeposited on the copper disc by submerging in 0.2 M $CuSO_4$ 1.5 M $H_2SO_{4(aq)}$, with and without polymer additives and applying a fixed cathodic current of 3 Acm^{-2} for 15 seconds. Polymer modified copper foam was synthesized by i) dissolving a mass of polymer corresponding to 10 mM concentration of the repeating monomer unit (excluding terminal -H groups), irrespective of polymer chain length, in the electrodeposition solution, or ii) dip-coating unmodified electrodeposited copper foam in 1.5 M $H_2SO_{4(aq)}$ solution of 10 mM (monomer) concentration of polymer for 30 seconds. The electrodeposited foams were submerged in deionized water for 1 minute to remove traces of electrodeposition solution prior to electrochemical measurements. For modification method ii, unmodified copper foam was submerged in deionized water for 1 minutes before being submerged into the polymer solution. The dip-coated copper foam was then submerged in deionized water for 1 minute to remove traces of acid and excess polymer. Full list of chemical reagents are listed in the ESI.

2.2 Material characterization

Scanning electron microscopic images were taken using SEM Bench-top TM3030 (Hitachi High-Technology Corporation, Japan). Energy dispersive X-ray spectroscopy was performed using AztecOne system (Oxford Instruments, UK) attached to the SEM, with an accelerating voltage of 5 kV and count number of 50,000. XPS was performed using the Kratos Axis Supra (Kratos Analytical, Japan) utilizing a monochromated Al Kα X-ray source, 15 mA emission current, magnetic hybrid lens and slot aperture. Region scans were performed using a pass

energy of 20 eV and step size of 0.1 eV. In-situ synchrotron X-ray diffraction measurements were performed at the ID03 beamline of the European Synchrotron Radiation Facility using X-ray wavelength of $\lambda = 0.641$ Å. Further details can be found in Fig S3.

2.3 CO_2 electrolysis

Potentiostat instruments CH440c (CH Instruments, USA) and Ivium-n-stat (Ivium Technologies B. V., Netherlands) were used for electrochemical measurements and electrolysis. Ivium-n-stat was used for electrochemical impedance spectroscopy for ohmic drop measurements, which was measured at a sinusoidal potential frequency of 10 kHz with 5 mV amplitude centered on the electrolysis potential just before electrolysis. 85% of the measured Ohmic drop was compensated for using the potentiostat control software, the remaining 15% (R_u) was manually adjusted for during data treatment using Ohm's law. Due to variations in ohmic drop and current between experiments, the actual potential difference also varied from run to run and so where relevant the potential is expressed as an average of at least three data points with the standard error shown as error bars. A three electrode set-up was used with a leak-free reference electrode based on Ag/AgCl in 3.4 M KCl (+0.21 V vs. SHE) (Innovative Instruments Inc., USA) and the counter electrode was a 2.5 cm * 5 cm piece of platinum mesh electrode (Goodfellow, UK). Potentials are converted to the reversible hydrogen electrode (RHE) scale using equation 1.

$$E_{\mathrm{RHE}} = E_{\mathrm{Ag/AgCl}} + \frac{2.303RT}{nF}pH + {E^0}_{\mathrm{Ag/AgCl}} - iR_{\mathrm{u}} \quad (1)$$

A custom-made H-cell was constructed from polypropylene body with 1.6 cm diameter and 7 cm length (Fig. S4), with a Nafion window (Nafion NRE-212 membrane, 0.05 mm thick, Alfa Aesar) which separates the working and reference electrodes from the counter electrode. Nitrogen or carbon dioxide gas was flowed into the electrolyte and maintained at a constant rate of at 40 $\mathrm{mlmin^{-1}}$ during electrolysis using a mass flow controller GFCS-010058

(Cole-Parmer, USA). A gas inlet and outlet stream were added to the cell to allow CO_2 to enter and escape while keeping the internal pressure of the cell at ambient levels. The outlet stream channel had a combined volume of ca. 40 ml, this was kept deliberately high to avoid suck back of air into the cell when headspace gas samples were taken using a gas-tight syringe (Hamilton company, USA) for injection into the sample loop of the gas chromatograph.

The electrolyte solution was prepared by saturating 0.05 M Na_2CO_3 with CO_2 by bubbling at >100 $mlmin^{-1}$ for an hour to form 0.1 M $NaHCO_3$ with a pH of 6.8. The electrolysis cell was saturated with CO_2 gas flowing at 40 $mlmin^{-1}$ for 5 minutes before cathodic potential was applied. Maintaining a flow of CO_2 into the electrolyte during electrolysis was crucial to achieving higher yields for carbonaceous products. No other method of liquid convection was employed, all reactions were carried out at room temperate, 25±2 °C. Electrolysis was carried out by setting the voltage at reducing potentials for a total of 35 minutes. Gas headspace samples were taken from the cell using a gas-tight syringe for manual injection into the GC sampling loop on the 5th, 20th and 35th minute. The electrolysis run was temporarily stopped after gas sample injection and the ohmic drop re-measured before starting the next segment. Running the segment up to the 20th and 35th minute was also repeated in constant current mode where the current was fixed to the average measured in the first 5 minutes, this would yield consistent results to potentiostatic electrolysis. Each set of gas phase product measurement was repeated at least three times, apart from the data point at -0.64 V vs. RHE which was only carried out once. Liquid phase products were quantified at the end of the 35 minute electrolysis run at a few selected potentials. Gaseous products were quantified using Agilent 7820A gas chromatograph (Agilent Technologies, UK), equipped with a thermal conductivity detector and flame ionization detector coupled to a methanizer. A dual column set-up was utilized, HP-PLOT Q and HP-PLOT 5A (Agilent Technologies, UK) for separation of hydrocarbons and permanent gases, respectively. Liquid phase products were quantified using Bruker AV-500 Nuclear Magnetic Resonance (NMR) Instrument.

Full details of methodologies are available in Fig. S5 and the accompanying text.

2.4 Theoretical calculations

First-principles calculations were performed within the density-functional-theory (DFT) formalism employing the Vienna Ab Initio Package (VASP)[31] with the Perdew-Burke-Ernzerhof (PBE)[32] exchange-correlation functional. The long-range dispersion correction to the PBE functional was introduced within the Grimme PBE-D3 approach.[33] The plane wave basis set cut-off energy was set to 400 eV. Brillouin zone integration was performed using a Monkhorst-Pack k-mesh of 4 x 4 x 1 and a Methfessel-Paxton smearing of 0.1 eV. Structural optimizations were conducted until the atomic forces were less than 0.03 eV/Å. Cu (100) and (111) surfaces were considered in the simulations, as the two gave the most intense XRD peaks in the copper foam samples. The surfaces were modelled using periodic slab model employing a 3 x 3 surface supercell and 5 metal layers separated by a vacuum gap of 15 Å. The solvation effect on CO dimerization in static calculations was accounted for by adding two solvent water molecules. The most energetically favorable atomic configurations of individual adsorbate pairs on the Cu surfaces were determined by running a series of geometry optimizations using different starting adsorption configurations and sites. Activation barriers for the CO dimerization reaction were determined using the climbing image NEB method.[34] Atomic charges were analyzed by the grid-based Bader analysis algorithm,[35] in which the grid is obtained by decomposition of the charge density via static self-consistent calculations for the optimized structures.

Ab initio molecular dynamics (AIMD) based simulations in conjunction with the Blue Moon ensemble technique were carried out at the Γ-point with explicit treatment of water environment at room temperature. The vacuum gap was filled with 45 H_2O molecules, equivalent to a water density of about 1 gcm^{-3}. Free-energy differences between initial and final states were calculated by integrating the averaged free energy gradients along the reac-

tion coordinate, defined as the distance between carbon atoms of neighboring CO molecules ($r_{oc\text{-}co}$). To drive the chemical reaction and generate a reaction path, we used the slow growth technique with an increment of 0.0005 Å/step. A set of windows along the reaction pathway was selected for thermodynamic integration. Configurations in each window were additionally equilibrated for 2 ps and simulations of 2-6 ps were carried out to collect and average the force along the reaction direction. The averaged gradients and corresponding free-energy profiles are presented later in the text. A similar computational scheme has been previously applied to examine CO_2 reactivity on the Cu (100) surface.[36]

3 Results and discussion

3.1 Material characterization

Table 1: Summary of electrochemically active surface areas of modified and unmodified copper foams, with corresponding surface roughness factors and current densities obtained from differential capacitance and CO_2 electrolysis measurements respectively. Applied potential difference: unmodified -0.98 V, poly(acrylamide) -0.96 V, poly(acrylic acid) -0.97 V, and poly(allylamine) -0.96 V, all vs. RHE.

	unmodified	poly(acrylamide)	poly(acrylic acid)	poly(allylamine)
Electrochemically active surface area (cm_2)	8.55 ± 0.83	11.5 ± 0.59	8.42 ± 0.94	44.8 ± 1.75
Surface roughness factor	121	162	119	634
$j_{geometric}$ ($mAcm^{-2}$)	55.4	60	65.8	147
j_{ECSA} ($mAcm^{-2}$)	0.458	0.37	0.553	0.232

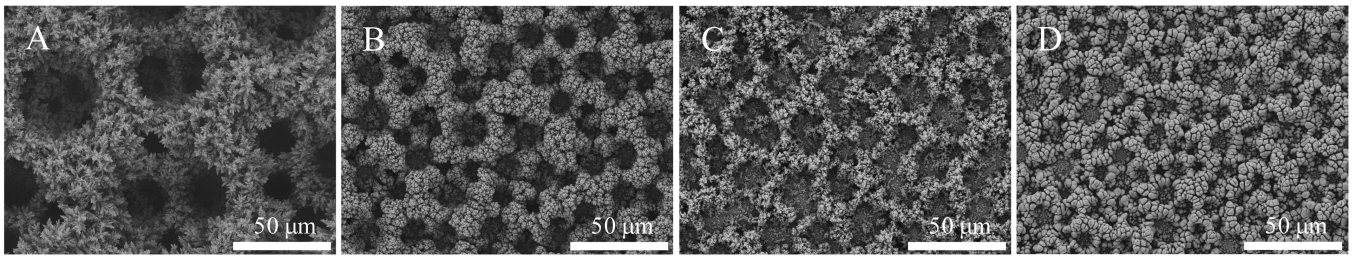

Figure 1: SEM images of copper foam electro-deposited with A) no additive, B) poly(acrylamide), C) poly(acrylic acid) and D) poly(allylamine)

As shown in the SEM images in Fig. 1, copper foam electrodeposited without additives have characteristic branching lamellar structures that have previously been reported.[37,38] Co-evolution of hydrogen bubbles cause a 'soft templating' effect where copper electrodeposits sparsely, leaving large pores as microstructures grow without fusing together.[38–40] This results in a significantly larger surface area being exposed to the electrolyte solution. The electrochemically active surface area is estimated by differential capacitance measurements in 0.1 M $HClO_4$.[41] However, we note that areas for modified foams are likely to be an underestimate as adsorbed polymer species may reduce the double layer capacitance from values reported for a pristine surface (see Fig. S6 and Table S3 for full results and further discussion). As shown in Table 1, copper foams deposited on a geometric surface area of 0.071 cm^2 has an electrochemically active surface area of 8.55 cm^2, this corresponds to a 121-fold increase in surface area. Despite utilizing electrodeposition conditions nearly identical to the one reported by Dutta et al., the copper foam was not black but appeared a dull red color similar to those reported by Sen et al. The color did not change even after exposure to air for over 24 hours. The electrochemical surface area is also nearly double that reported by Dutta et al., and the activity for CO_2 reduction is also different as will be discussed later.

Addition of poly(acrylamide), poly(acrylic acid) and poly(allylamine) changes the morphology of the copper foams. Growth of hierarchical copper structures in the presence of additives is a complex process which involves dendrite growth suppression by adsorption of the polymer on the copper.[42,43] Such additives may also affect soft templating by control of hydrogen bubble coalescence.[44–46] The cited studies used different additives such as poly(ethylene glycol), $(NH_4)_2SO_4$ and benzotriazole but report similar morphologies to those in Fig. 1. Electrodeposited copper in the presence of poly(acrylamide) and poly(allylamine) (Fig. 1B and 1D respectively) have more rounded and compact structures due to dendrite growth inhibition via polymer adsorption. Addition of poly(acrylic acid) results in thinner dendritic copper film which suggests a greater extent of copper growth suppression. It is im-

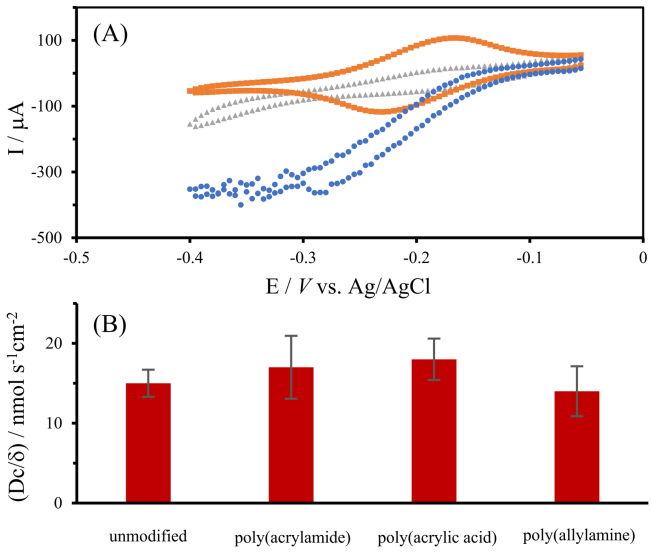

Figure 2: A) Cyclic voltammograms recorded at $10 mVs^{-1}$ in 0.1 M $NaHCO_3$ with argon flow at 40 $mlmin^{-1}$ (grey △), with same rate of argon flow and 10 mM $Ru(NH_3)_6Cl_3$ (blue ○), and 10 mM $Ru(NH_3)_6Cl_3$ without argon flow (orange □). B) Equivalent hydrodynamic flux calculated from steady state reduction currents for $Ru(NH_3)_6Cl_3$ under constant argon flow, see Fig. S7 for full experimental results. Error bars show error from steady state current measurements.

portant to consider the meso and micro-scale morphology of the copper foam, as it can affect mass transport and pH conditions inside the material which can affect its catalytic activity and selectivity.[47] Relative rates of mass transport in foam structures are quantitatively gauged through voltammetry of redox probe $Ru(NH_3)_6Cl_3$ under experimental conditions identical to CO_2 electrolysis but with CO_2 gas flow substituted with argon gas. The dependence of peak cathodic current on the square root of scan rate in the absence of argon gas flow shows that $Ru(NH_3)_6Cl_3$ reduction is mass-transport limited (Fig. S7). When the electrolyte solution is agitated by argon bubbling, a hydrodynamic pseudo-steady state current is established (at 10 mVs^{-1}). The average diffusion layer thickness can be estimated from the steady state current ($I_{s.s.}$), and from this the average hydrodynamic flux of the electroanalyte is found from Dc/δ in units of $mols^{-1}cm^{-2}$, D is the diffusion coefficient of the electroanalyte (cm^2s^{-1}), c is concentration in ($molcm^{-3}$) and δ is the diffusion layer thickness in cm. As shown in Fig. 2B, the average hydrodynamic flux (in the limit of 1-D mass transport) across

four different foam materials fall within a similar range (full details can be found in Fig. S7). Hence, despite the difference in material morphology, similar mass-transport conditions are established in the electrolyte by bubbling gas at a fixed rate of 40 mlmin^{-1}.

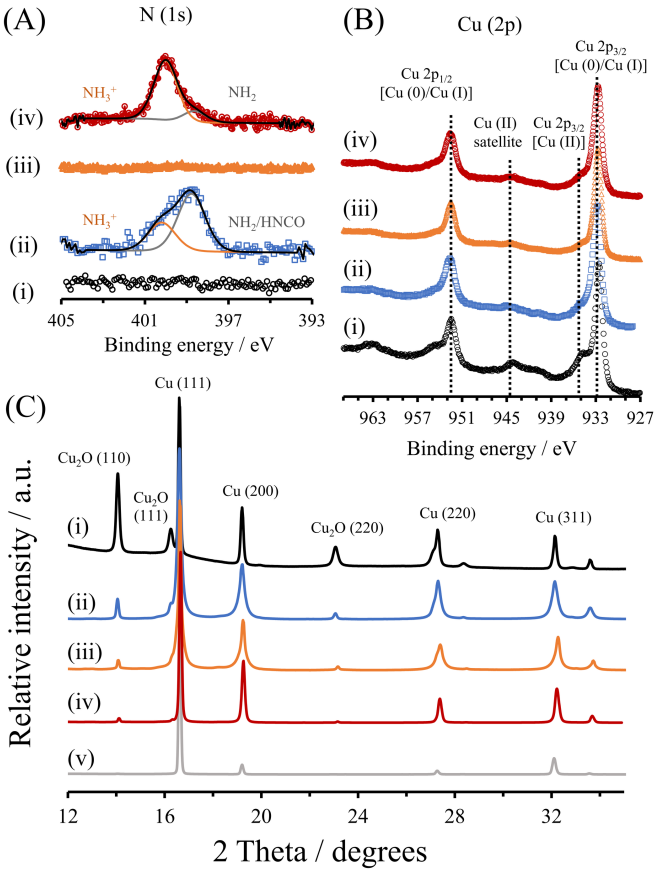

Figure 3: Ex-situ X-ray photoelectron spectra of A) N(1s) and B) Cu(2p) regions. C) Ex-situ grazing angle synchrotron X-ray diffractograms. Copper foams electrodeposited with i) no additive, ii) poly(acrylamide), iii) poly(acrylic acid) and iv) poly(allylamine). v) polycrystalline copper.

X-ray photoelectron spectra of the copper surface in Fig. 3A reveals the presence of nitrogen only for copper foams electrodeposited with poly(acrylamide) and poly(allylamine). Post-electrolysis XPS measurements in Fig. S8 show that nitrogen peaks remain unchanged, indicating that the amines are stable during electrolysis. The presence of both copper metal and copper oxide in the Cu (2p) and Cu LMM spectra (Fig. S8) implies that the surface oxide layer is present at nanometer scale thickness (XPS probing depth). Electrodeposition of

copper in acidic conditions yields Cu(0),[48] but the surface can be readily oxidized by contact with air or water to form a shell of oxides. EDX analysis in Fig. S9 (which probes a depth of microns) shows that oxygen and nitrogen are present in lower concentration when compared to XPS data. While it is known that electrodeposition additives can deposit between grain boundaries that permeate the bulk material,[49] in the case of nitrogen, XPS data shows it is 5-8 times more concentrated when compared to EDX data. This suggests that polyamines are not homogeneously deposited in the bulk copper structure but adsorbed on the surface. Qualitative comparisons of the ex-situ grazing angle synchrotron XRD data in Fig. 3C shows that unmodified copper foam has the thickest layer of Cu_2O, with a Cu (111) : Cu_2O (110) peak ratio of 1 : 0.73, which is significantly larger than for polymer modified foams which has a ratio of around 1 : 0.1. This may suggest that adsorbed polymers suppress formation of copper oxides, as reported for various modifiers and electrodeposition additives such as octadecylamine and cysteine.[50,51] All copper foams are poly-crystalline and have peaks corresponding to Cu_2O. The relative intensity for Cu (111) : Cu (200) are similar for all copper foams at 1 : 0.44. Cu (111) : Cu (220) ratio is highest for unmodified copper at 1 : 0.5, while all modified foams has as a ratio of 1 : 0.3. Cu (111) : Cu (311) peak ratio is consistent across all foams at 1 : 0.3. The similarities in crystalline phase distribution in modified copper foams suggests that the polymer additives do not adsorb onto specific sites for preferential inhibition of crystalline phases.

3.2 CO_2 electrolysis

As shown in figure 4, unmodified copper foam produces ethylene with a faradaic efficiency of 13%, which is significantly higher than the 2% previously reported by Sen et al.[18] Sen saturated the electrolyte prior to electrolysis but did not have a constant flow of CO_2 agitating the solution. Preliminary experiments on unmodified copper foams under similar conditions (without constant flow of CO_2) yielded similar levels of hydrocarbons (Fig. S10). As the

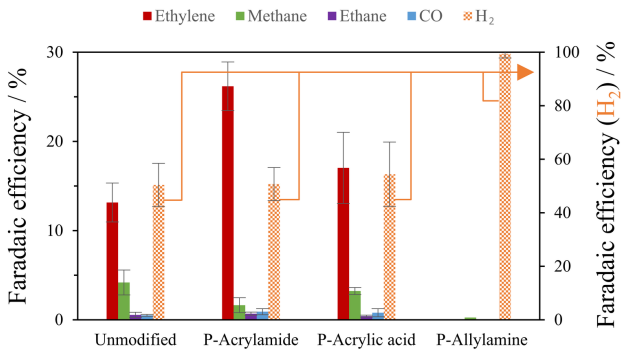

Figure 4: Bar chart of faradaic efficiencies of copper foams modified with additives for CO_2 reduction. Electrolysis carried out in 0.1 M $NaHCO_{3(aq)}$ at ca. -0.96 V vs. RHE for 35 minutes. See Table 1 for current densities and applied potentials. Error bars show ± 1 standard error.

total faradaic charge passed equates to only a small fraction of the total CO_2 dissolved in the electrolyte, this suggests that maintaining high rates of mass transport of CO_2 to the electrode surface is crucial to achieving higher faradaic efficiencies for hydrocarbons, this was also noted by Kuhl et al. for copper foil electrodes.[52] Copper foam deposited in presence of poly(acrylamide) results in the faradaic efficiency for ethylene doubling to 26%. To the best of our knowledge, this results in the highest reported partial current density for hydrocarbons at 21.2 $mAcm^{-2}$ at -1.05 V vs. RHE for catalysts based in aqueous sodium/potassium bicarbonate electrolyte. The increase in selectivity for hydrocarbons on poly(acrylamide) modified copper cannot simply be attributed to mass transport of CO_2, given that mass transport conditions in poly(acrylamide) modified copper foam is estimated to be similar to unmodified foam based on earlier discussion related to Fig. 2. Poly(acrylamide) modified copper foam exhibits slightly lower CO_2 electrolysis current density (ECSA normalized) than unmodified foam (see Table 1). Assuming that a proton is consumed for every electron transferred, the surface pH is expected to be higher on unmodified copper foam under CO_2 electrolysis conditions. This should favor higher selectivity for ethylene based on pH effects studied by Gupta et al.,[47] but this is not what is observed in experiments. While modification with poly(acrylic acid) shows a slight enhancement in faradaic efficiency, the performance of the electrode decays rapidly as a function of electrolysis time (Fig. S11). Poly(allylamine)

almost completely inhibits CO_2 reduction in favor of the hydrogen evolution reaction. This also cannot be explained purely based on pH or mass transport effects, but is likely to be a chemical effect from the adsorbed polymer, similar to Hori's observation of the inhibitory effect trimethylamine had on copper electrocatalysts.[53]

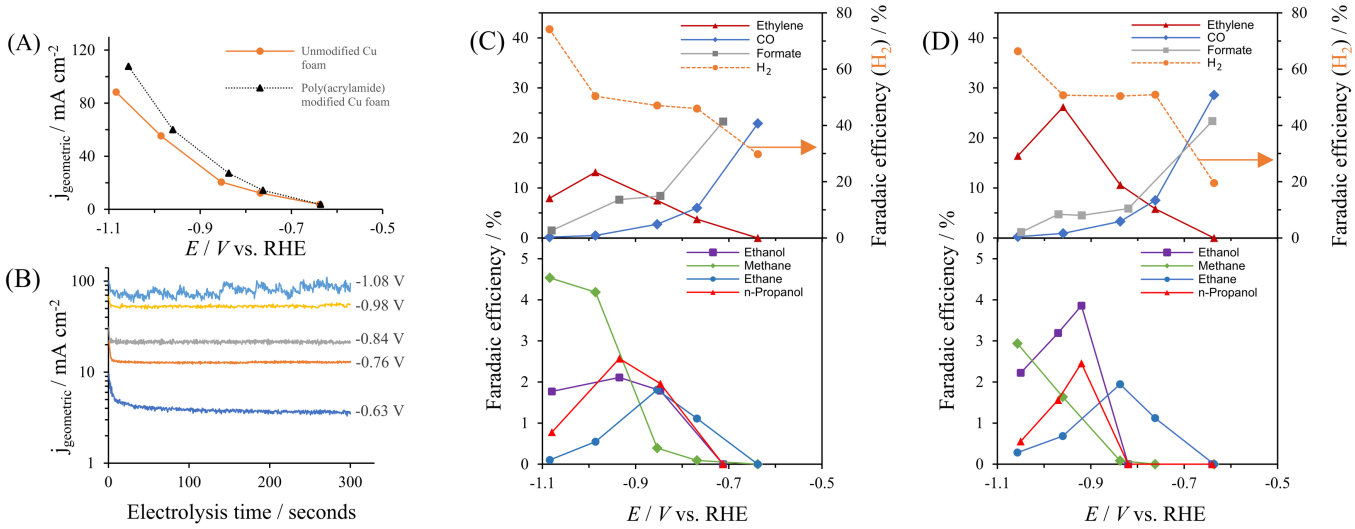

Figure 5: A) Geometric current densities of copper foam unmodified and modified with poly(acrylamide), B) Initial segment of the chronoamperogram of CO_2 electrolysis on unmodified copper foam in 0.1 M $NaHCO_3$ at varying potentials, C) Faradaic efficiency versus applied potential for unmodified copper foam and D) same as C but for copper foam modified with poly(acrylamide). See Fig. S12 for error bars.

A broader range of potentials are studied to further investigate the enhancement of faradaic efficiency caused by poly(acrylamide) modification. The faradaic efficiency for carbon monoxide on unmodified copper foam starts off at 23% and decreases to nearly zero at more negative potentials following a similar trend to that of copper foil as benchmarked by Kuhl et al.[52] Formate is produced at faradaic yields similar to copper foil at ca. 20%, but it starts to decrease at an earlier potential of around -0.7 V vs. RHE (compared to -0.9 V for copper foil). Hydrocarbons also follow a similar trend up to -0.98 V vs. RHE except with the geometric current density being much higher (at 55 mAcm^{-2} compared to 1.9 mAcm^{-2} for copper foil). Ethylene evolution is observed before methane and the faradaic efficiency is also

at similar values of 13% for ethylene and 4% methane at -0.98 V vs. RHE. The trend breaks at -1.08 V, where there is a decrease in faradaic efficiency to 8% for ethylene, and methane only slightly increases to 4.5%, whereas copper foil performs with faradaic efficiencies of 21.4% and 30% for ethylene and methane respectively. The observed difference in selectivity at -1.08 V vs. RHE may arise from CO_2 mass transport limitations at high current density (of 88 $mAcm^{-2}$), as opposed to intrinsic selectivity of the foam electrode. To achieve the same faradaic efficiencies for hydrocarbons at 88 $mAcm^{-2}$, CO_2 flux to the electrode surface must reach 50 nmol $s^{-1}cm^{-2}$. This is equivalent to the flux generated by a disc electrode rotating at 470 rpm, using the Levich equation[54] ($C_{CO2} = 0.0341$ M and $D_{CO2(aq)} = 2 \times 10^{-6}$ cm^2s^{-1}, kinematic viscosity = 0.0102 cm^2s^{-1}). Given the flux of gaseous products coming out of the porous copper foam below -1.0 V (which is high enough to distort chronoamperometric measurements as shown in Fig. 5B), mass transport of CO_2 into the pores is likely to be impeded. This results in the increase of hydrogen evolution at more negative potentials compared to copper foil electrodes. Ethanol and n-propanol follows a similar trend as on copper foil but the faradaic efficiency for ethanol is significantly lower at 2% whereas on foil just under 10% is reported. Unlike copper foil, foam also produces a small amount of ethane (less than 2%). A recent study found that mesopores (2-50 nm) can favor ethane as the dominant product as its isolated environment offers different pH and intermediate dwell times compared to larger pores and open surfaces.[55] This may also explain why the ethane yield does not increase upon increased mass transport of CO_2 as mesopores may be shielded from solution convection (see Fig. S10). This is in contrast to ethylene and carbon monoxide, suggesting that these products predominantly form on different copper sites that can benefit from the increased mass transport of CO_2.

The increase in geometric current for poly(acrylamide) modified copper foam compared to unmodified foam as shown in Fig. 5A is expected with the increase in electrochemically active surface area. The faradaic current may not scale linearly with surface area due to

significant diffusion layer overlap in porous films. The largest change in product selectivity from poly(acrylamide) modification can be observed for ethylene which reaches a maximum faradaic efficiency of 26% at -0.96 V (vs. RHE), this is double that of unmodified copper foam. The faradaic efficiency for ethanol also doubles, though this is still at only 4%. There is also a slight increase of CO from 23% on unmodified to 29%. Faradaic efficiencies for ethane, n-propanol and hydrogen remain similar while there is a slight decrease in methane production. Longer duration electrolysis experiments (shown in Fig. S11) shows that the faradaic efficiency for hydrogen increases up to 55% for unmodified copper after 1 hour at -0.98 V vs. RHE, whereas poly(acrylamide) modified copper remains at a stable value. While the magnitude of faradaic efficiencies is different, the trends appear to remain similar. Due to the high gas flow rate chosen for optimal mass transport, the limit of quantification at more positive potentials (lower current) is rather high, which makes accurate determination of onset potentials difficult (see Fig. S13). However, the increased selectivity for C_2 products here is noteworthy. This cannot be explained by mass transport or pH effects, and given that the distribution of crystalline phases in all copper foams are similar, additional factors need to be considered to account for the enhanced catalytic kinetics. The following sections will consider i) presence of oxide derived copper, and ii) stabilization of reaction intermediates by functional groups on the polymer.

3.3 In-situ synchrotron XRD

In-situ XRD measurements in Fig. 6 show that the Cu_2O peaks decay as a function of applied (reductive) potentials, and disappear completely at CO_2 electrolysis conditions. The decay of the Cu_2O (110) peak appears to be independent of the additives used to modify the copper. Ren et al. reported similar trends of rapid copper oxide reduction under CO_2 electrolysis conditions using in-situ Raman spectroscopy.[56] Kas et al. also reported that no carbonaceous products could be detected using online mass spectrometry on copper oxide

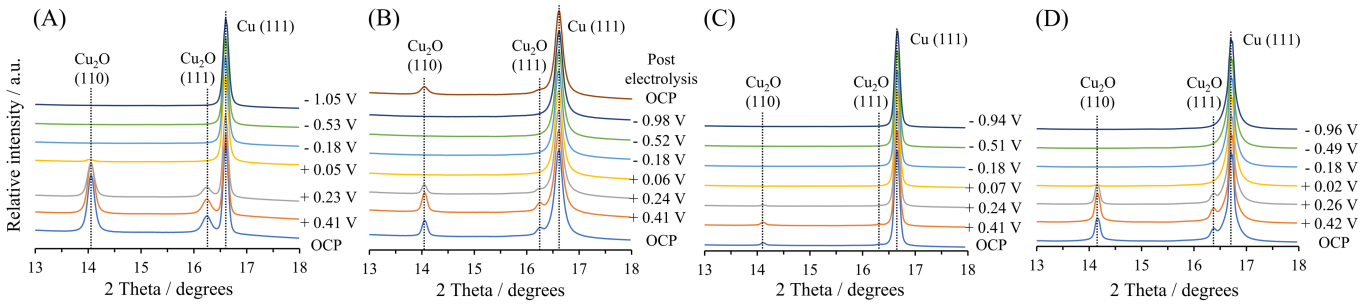

Figure 6: In-situ grazing angle X-ray diffractograms of copper foams modified with A) no additive, B) poly(acrylamide), C) poly(acrylic acid), and D) poly(allylamine). Copper foams were immersed in aqueous 0.1 M $NaHCO_3$ saturated with CO_2, all potentials reported vs. RHE.

surfaces.[9] While the presence of residual amorphous surface oxides under CO_2 electrolysis conditions cannot be discounted based only on the in-situ XRD data, current evidence suggest that oxides are unlikely to be the active material responsible for the enhanced catalysis of CO_2 reduction. Studies on surface adsorbed copper corrosion inhibitors speculate on the presence of Cu^+ species stabilized by coordination with the adsorbed inhibitor.[50,51,57] We cannot discount the presence of such complexes on modified copper foam. However, it is difficult to rationalise the enhanced kinetics of CO_2 through such surface species as the stability of Cu^+ is dependent on coordination to the inhibitor, which makes it unavailable for binding CO_2 reduction intermediates.

The uppermost diffractogram in Fig. 6B, recorded at open circuit potential one hour after complete reduction of oxides, shows that metallic copper readily oxidizes to Cu_2O when exposed to electrolyte solution. Freshly prepared and dried unmodified copper foams had the most intense XRD peak for Cu_2O relative to metallic copper, but itś catalytic selectivity for CO_2 reduction products was similar to metallic copper foil. The black copper foams recently investigated by Dutta has very different selectivity for CO_2 reduction with faradaic efficiencies of 30% for ethane and 20% for ethylene at -0.9 V vs. RHE, and complete suppression of methane formation.[20] Dutta attributes the difference in product selectivity to copper oxidized by room-temperature air, which reduces to oxide derived copper in-situ un-

der CO_2 electrolysis conditions. While increase in selectivity for ethane up to 10% faradaic efficiency has previously been reported for oxide derived copper catalysts, this was achieved by electrodepositing oxides in highly basic copper sulfate solution with lactates additives,[9,10] treating copper foil with oxygen plasma,[58] or heating at 300 °C for 30 minutes or longer or at higher temperatures.[7] Such treatment would typically result in Cu_2O films that is estimated to be around 1-3 microns thick assuming bulk density for Cu_2O. While there is some debate over the precise chemical nature of the active phase in oxide derived copper,[59,60] the heat treatment study by Li et al. found a systematic increase in the yield of carbonaceous products with the initial thickness of Cu_2O layer. The cited studies also found that there was a significant shift in CO onset potential 0.2 V more positive compared to metallic copper (the whole faradaic efficiency vs. potential plot appears to shift). In the case of thermal annealing and plasma treatment, onset potential of ethylene also shifted 0.1 V and 0.25 V more positive, respectively. Given that the oxide layers on both modified and unmodified copper foam studied here are estimated to be nanometers thick (based on XPS data), and the trend of CO and ethylene evolution has not changed significantly, the enhancements in catalytic activity observed from poly(acrylamide) modified copper compared to unmodified is not consistent with copper oxide derived catalysts.

3.4 Density functional theory calculations: effect of adsorbed poly(acrylamide)

We consider the effect of adsorbed polyamines by investigating unmodified copper foam that is dip-coated in poly(acrylamide) after electrodeposition for CO_2 electrolysis. As shown in Fig. 7, the modification results in an enhancement in selectivity for C_2 electrolysis products that is very similar to the results obtained for copper foams electrodeposited in presence of poly(acrylamide). As the dip-coating procedure is carried out in ambient pressure and temperature, the distribution of crystalline phases and level of oxides present on the copper foam is expected to be unchanged. With nearly identical structural morphology and reac-

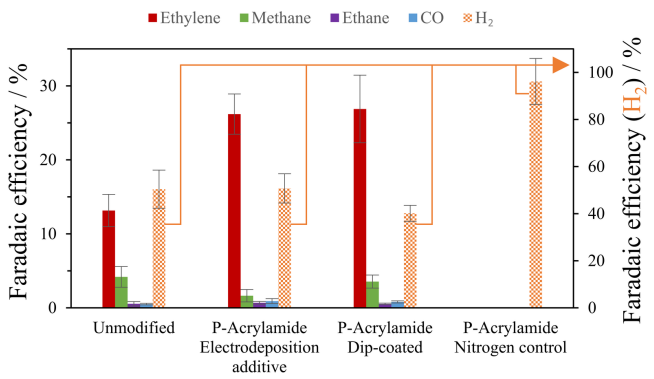

Figure 7: Bar chart of faradaic efficiencies of copper foams for CO_2 reduction. Electrolysis carried out for 35 minutes in 0.1 M $NaHCO_{3(aq)}$. Copper foam with no additive (55.4 $mAcm^{-2}$ at -0.98 V), poly(acrylamide) electrodeposition additive (60 $mAcm^{-2}$ at -0.96 V), poly(acrylamide) dip-coated (50.4 $mAcm^{-2}$ at -0.99 V) and poly(acrylamide) electrodeposition additive but with nitrogen flow (70 $mAcm^{-2}$ at -0.95 V), all vs. RHE. Error bars show $\pm$ 1 standard error.

tion conditions, pH is also expected be similar under electrolysis conditions. This strongly suggests that the enhancement in CO_2 reduction products is due to the presence of the poly(acrylamide) group on the electrode surface. Control experiments with poly(acrylamide) modified copper foam where nitrogen gas is flowed through the cell during electrolysis instead of CO_2 yields only hydrogen gas, which unambiguously shows that the observed carbonaceous products are due to enhanced CO_2 reduction kinetics as opposed to contamination effects or polymer degradation.

A series of first-principles simulations are carried out to obtain insights into the chemical and electronic effects poly(acrylamide) modification offers copper for improved selectivity toward C_2 products. Static DFT calculations show that acrylamide (CH_3-CO-NH_2) monomer strongly binds to the copper surface via the oxygen atom of the CO group. Specifically, the energies for acrylamide monomer are -0.42 eV and -0.47 eV on Cu (100) and Cu (111) surfaces, respectively. The binding energy of acrylamide oligomer (CH_x-CO-NH_2)$_4$ are computed to be even higher, at -2.05 eV and -2.32 eV for the Cu (100) and Cu (111) surfaces, respectively. Thus, both surfaces are expected to be partially covered by acrylamide oligomer, while va-

cant surface sites are available for CO_2 adsorption and subsequent reduction reactions. The adsorption and inhibitive effect of poly(allylamine) which does not contain carbonyl groups must follow a different mechanism, possibly adsorbing on copper through the nitrogen atom and enhancing the hydrogen evolution reaction by acting as a proton shuttler.[61,62]

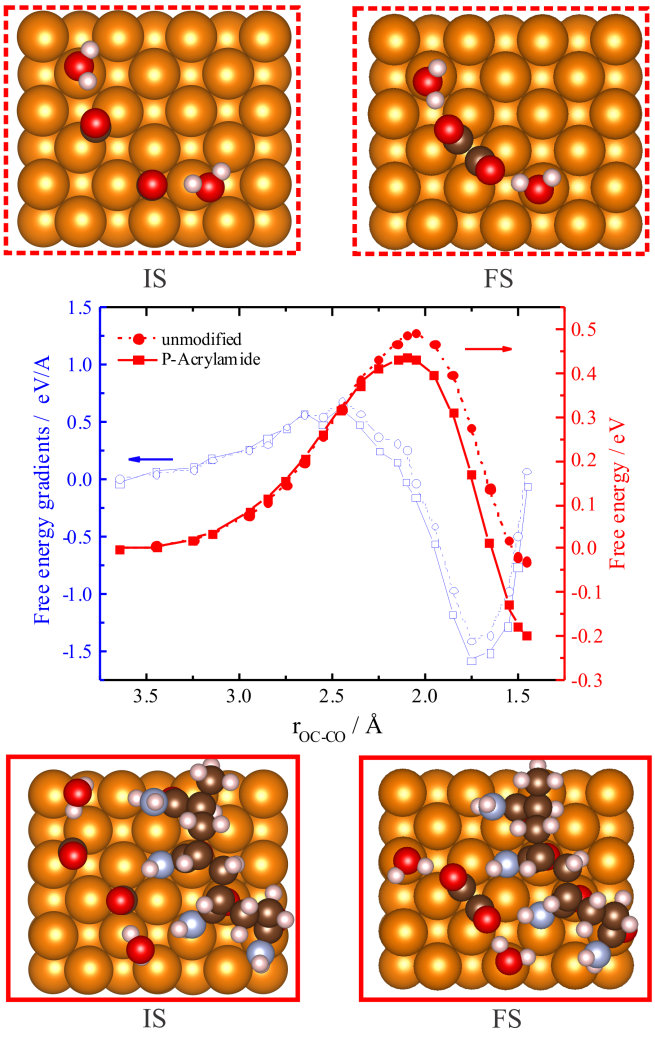

Figure 8: Free energy gradients (left-hand scale) and corresponding free energy profiles (right-hand scale) for the CO dimerization reaction on unmodified and poly(acrylamide) modified Cu (100) surfaces as obtained from AIMD based Blue Moon ensemble simulations. IS and FS stands for initial and final states, respectively. The distance between carbon atoms of neighboring CO molecules ($r_{oc\text{-}co}$) is used as a reaction coordinate. Only two nearest H_2O molecules are shown, while the remaining solution H_2O are omitted for clarity.

Prior investigations suggest that CO dimerization is the key step leading to the forma-

tion of C_2 products.[36,63–65] Here, we model CO dimerization with and without acrylamide molecules on the copper surface. It was previously shown that explicit treatment of the solvent could impact the dynamics and kinetics of various CO_2 conversion reactions.[66] Here, ab initio molecular dynamics (AIMD) simulations in combination with the Blue Moon ensemble approach is used to accurately evaluate the activation barriers of CO dimerization reaction in an explicit water environment at room temperature. A similar computational approach was previously applied to examine CO_2 reactivity on Cu (100).[36]

Fig. 8 shows the free-energy profiles for CO dimerization over the Cu (100) surface with and without acrylamide oligomer. The presence of acrylamide on the surface results in a 0.06 eV decrease of the dimerization activation barrier and stabilization of the formed dimer by almost 0.2 eV. We note that the position of CO molecules on Cu (in solution at room temperature) may vary and should also depend on CO surface coverage. Additional static CNEB calculations show that if both CO molecules are placed at the bridge positions on Cu, this leads to a more pronounced decrease of the activation barrier (0.18 eV) for the acrylamide modified copper surface, compared to the AIMD based results (Fig. S14). Overall, the computed activation barriers of CO dimerization on unmodified Cu (100) are found to be in agreement with previous studies that reported values ranging from 0.33 eV to 0.69 eV depending on the employed model.[36,63,64,66] CNEB calculations also show that Cu (111) surface has a larger barrier for CO dimerization even in the more favorable case of acrylamide-modified Cu (111) at ca. 0.6 eV, thus the Cu (100) facet should exhibit higher efficiency for ethylene formation. This is in agreement with previously reported experimental,[11,12] and theoretical studies,[65,66] hence the observed increase in ethylene production is mainly attributed to the activity of the Cu (100) facet.

Bader charge density analysis shows that adsorption of acrylamide oligomer on the Cu (100) surface activates the adsorbed CO molecules through modification of the surface po-

tential. Specifically, modification of Cu with poly(acrylamide) causes the surface charge to become more negative by 0.21e compared to the unmodified surface. As indicated by the electron density difference map in Fig. S15, co-adsorption of two CO molecules with acrylamide oligomer leads to charge transfer from the surface to the adsorbed CO molecules (0.11e on each) causing hybridization. This facilitates dimerization with a lowered activation barrier. A similar effect was observed by Ogura and co-workers who demonstrated that copper mesh electrode modified by copper(I) halides (CuBr, CuCl or CuI) increased the faradaic efficiency of ethylene formation compared to pure copper mesh due to the adsorption of halide anions on the surface.[67,68] We also note that the -NH_2 group on the oligomer contributes to the stabilization of the dimer by H-bonding.

Our calculations also reveal that oligomer modification of the Cu (100) surface not only decreases the activation barrier of CO dimerization, but also facilitates the adsorption of CO molecules in the vicinity of the oligomer (binding energy of -0.98 eV without and -1.25 eV with the oligomer). This should lead to higher concentrations of adsorbed CO on copper close to acrylamide oligomers, which can also contribute to enhanced dimerization.[64,69] All three stabilizing effects from the polymer identified by theoretical simulations are localized effects, hence cannot be mediated by trace additives that may be embedded in the bulk material. The decrease in CO dimerization barrier and increased local coverage of CO offered by poly(acrylamide) adsorption on the copper surface help explain the increased yield of ethylene observed in experiments. This also sheds some light on the case of poly(acrylic acid) modified copper, where an initial increase in faradaic yield for ethylene of 19% at -0.97 V vs. RHE was observed (see Fig. S11). Given the similarities in chemical structure with poly(acrylamide), the above mentioned effects may also play a role in enhancing kinetics of ethylene formation. But with poly(acrylic acid), the -OH group is deprotonated ($pK_a = 4.5$) hence the stabilization effect from hydrogen-bonding interactions is absent. The proposed mechanism for enhanced catalytic kinetics presented here contrasts from previous work by

Xie et al. on amino acid (monomer) modified copper, where -NH_3^+ species were considered as the active functional group stabilizing CO_2 reduction intermediates via 'a strong hydrogen-bond like interaction'. Given that the surface of the copper electrode during CO_2 electrolysis is expected to be in the pH region of 9.8-10.8 (depending on current density), the amine group on glycine with a pK_a of 9.6 is unlikely to be protonated. This work also differs as polymers were studied instead of monomers, further work needs to be carried out to understand the effect of polymer chain length.

4 Conclusions

In summary, modification of the copper foam surface with poly(acrylamide) doubles the faradaic yield of ethylene with high geometric partial current density for hydrocarbons (>20 $mAcm^{-2}$). Poly(acrylic acid) also shows a similar effect that is short lived, whereas poly(allylamine) completely inhibits CO_2 reduction. DFT calculations reveal that poly(acrylamide) adsorbs on copper via the oxygen on the carbonyl groups, and enhances the efficiency of ethylene formation by i) charge donation to the copper surface that activates CO for dimerization, ii) chemical stabilization of the CO dimer (a key intermediate for C_2 products) by hydrogen-bond interactions with the -NH_2 group, and iii) facilitating the adsorption of CO molecules near the polymer, increasing local surface coverage. Further enhancement of ethylene formation should be achievable with porous copper catalysts rich in Cu (100) crystals, high CO_2 mass transport in the pore structure, and modification with poly(acrylamide). Due to fundamental limits with optimizing multi-step electron transfer reactions on catalysts with non-optimal 'scaling relations' between reaction intermediates, it is envisioned that the next generation of heterogeneous CO_2 reduction catalysts will host multi-point binding sites as ubiquitously found in nature (i.e. enzymes with 3D active sites). Poly(acrylamide) modified copper demonstrates such a case, where the adsorbed polymer activates and stabilize reac-

tion intermediates through novel mechanisms proposed in this study.

5 Author information

The authors declare no competing financial interest.

Supporting Information Available

The following files are available free of charge.

- Filename: Copper-polymer-SI

  Contains additional data, analysis and references.

This material is available free of charge via the Internet at `http://pubs.acs.org/`.

Acknowledgement

Financial support was provided by the Engineering and Physical Sciences Research Council (EPSRC) Research Grant EP/N009525/1, and the Welsh Government Sêr Cymru Program. This work is also part of the Flexible Integrated Energy Systems (FLEXIS) research operation, which is partly funded by the European Regional Development Fund (ERDF), through the Welsh Government. We acknowledge the European Synchrotron Radiation Facility for provision of synchrotron radiation facilities (beamline ID03 under proposal number MA-3335). We thank J. C. Romero Torrecilla for technical and instrumental assistance. R. J. Wakeham is supported by funding from the European Union Horizon 2020 research and innovation program under the Marie Skłodowska-Curie grant agreement No 663830. This research used computational resources of the National Energy Research Scientific Computing Center, a DOE Office of Science User Facility supported by the Office of Science of the

U.S. Department of Energy under Contract No. DE-AC02-05CH11231, and the Holland Computing Center at the University of Nebraska-Lincoln. All data created during this research are openly available from the Swansea University Open Research Data archive at https://doi.org/10.5281/zenodo.1183430.

References

(1) Senftle, T. P.; Carter, E. A. The Holy Grail: Chemistry Enabling an Economically Viable CO_2 Capture, Utilization, and Storage Strategy. *Acc. Chem. Res.* **2017**, *50*, 472–475.

(2) Martens, J. A.; Bogaerts, A.; De Kimpe, N.; Jacobs, P. A.; Marin, G. B.; Rabaey, K.; Saeys, M.; Verhelst, S. The Chemical Route to a Carbon Dioxide Neutral World. *ChemSusChem* **2017**, *10*, 1039–1055.

(3) Hori, Y.; Kikuchi, K.; Suzuki, S. Production of CO and CH_4 in electrochemical reduction of CO_2 at metal electrodes in aqueous hydrogencarbonate solution. *Chem. Lett.* **1985**, *11*, 1695–1698.

(4) Kuhl, K. P.; Hatsukade, T.; Cave, E. R.; Abram, D. N.; Kibsgaard, J.; Jaramillo, T. F. Electrocatalytic conversion of carbon dioxide to methane and methanol on transition metal surfaces. *J. Am. Chem. Soc.* **2014**, *136*, 14107–14113.

(5) Liu, X.; Xiao, J.; Peng, H.; Hong, X.; Chan, K.; Nørskov, J. K. Understanding trends in electrochemical carbon dioxide reduction rates. *Nat. Commun.* **2017**, *8*, 15438.

(6) Peterson, A. A.; Nørksov, J. K. Activity Descriptors for CO_2 Electroreduction to Methane on Transition-Metal Catalysts. *J. Phys. Chem. Lett.* **2012**, *3*, 251–258.

(7) Li, C. W.; Kanan, M. W. CO_2 reduction at low overpotential on Cu electrodes resulting from the reduction of thick Cu_2O films. *J. Am. Chem. Soc.* **2012**, *134*, 7231–7234.

(8) Kim, D.; Lee, S.; Ocon, J. D.; Jeong, B.; Lee, J. K.; Lee, K.; Lee, J. K. Insights into autonomously formed oxygen-evacuated Cu_2O electrode for the selective production of C_2H_4 from CO_2. *Phys. Chem. Chem. Phys.* **2014**, *17*, 1–9.

(9) Kas, R.; Kortlever, R.; Milbrat, A.; Koper, M. T. M.; Mul, G.; Baltrusaitis, J. Electrochemical CO_2 reduction on Cu_2O-derived copper nanoparticles: controlling the catalytic selectivity of hydrocarbons. *Phys. Chem. Chem. Phys.* **2014**, *16*, 12194–201.

(10) Handoko, A. D.; Ong, C. W.; Huang, Y.; Lee, Z. G.; Lin, L.; Panetti, G. B.; Yeo, B. S. Mechanistic Insights into the Selective Electroreduction of Carbon Dioxide to Ethylene on Cu_2O-Derived Copper Catalysts. *J. Phys. Chem. C* **2016**, *120*, 20058–20067.

(11) Hori, Y.; Takahashi, I.; Koga, O.; Hoshi, N. Selective formation of C_2 compounds from electrochemical reduction of CO_2 at a series of copper single crystal electrodes. *J. Phys. Chem. B* **2002**, *106*, 15–17.

(12) Schouten, K., Gallent, E., Koper, M. Structure Sensitivity of the Electrochemical Reduction of Carbon Monoxide on Copper Single Crystals. *ACS Catal.* **2013**, *3*, 1292–1295.

(13) Zall, C. M.; Linehan, J. C.; Appel, A. M. A Molecular Copper Catalyst for Hydrogenation of CO_2 to Formate. *ACS Catal.* **2015**, *5*, 5301–5305.

(14) Weng, Z.; Jiang, J.; Wu, Y.; Wu, Z.; Guo, X.; Materna, K. L.; Liu, W.; Batista, V. S.; Brudvig, G. W.; Wang, H. Electrochemical CO_2 Reduction to Hydrocarbons on a Heterogeneous Molecular Cu Catalyst in Aqueous Solution. *J. Am. Chem. Soc.* **2016**, *138*, 8076–8079.

(15) Manthiram, K.; Beberwyck, B. J.; Alivisatos, A. P. Enhanced electrochemical methanation of carbon dioxide with a dispersible nanoscale copper catalyst. *J. Am. Chem. Soc.* **2014**, *136*, 13319–13325.

(16) Reske, R.; Mistry, H.; Behafarid, F.; Roldan Cuenya, B.; Strasser, P. Particle size effects in the catalytic electroreduction of CO_2 on Cu nanoparticles. *J. Am. Chem. Soc.* **2014**, *136*, 6978–6986.

(17) Loiudice, A.; Lobaccaro, P.; Kamali, E. A.; Thao, T.; Huang, B. H.; Ager, J. W.; Buonsanti, R. Tailoring Copper Nanocrystals towards C_2 Products in Electrochemical CO_2 Reduction. *Angew. Chem. Int. Ed.* **2016**, *55*, 5789–5792.

(18) Sen, S.; Liu, D.; Palmore, G. T. R. Electrochemical Reduction of CO_2 at Copper Nanofoams. *ACS Catal.* **2014**, *4*, 3091–3095.

(19) Deciccio, D.; Ahn, S. T.; Sen, S.; Schunk, F.; Palmore, G. T. R.; Rose-Petruck, C. Electrochemical reduction of CO_2 with clathrate hydrate electrolytes and copper foam electrodes. *Electrochem. Commun.* **2015**, *52*, 13–16.

(20) Dutta, A.; Rahaman, M.; Luedi, N. C.; Mohos, M.; Broekmann, P. Morphology Matters: Tuning the Product Distribution of CO_2 Electroreduction on Oxide-Derived Cu Foam Catalysts. *ACS Catal.* **2016**, *6*, 3804–3814.

(21) Reller, C.; Krause, R.; Volkova, E.; Schmid, B.; Neubauer, S.; Rucki, A.; Schuster, M.; Schmid, G. Selective Electroreduction of CO_2 toward Ethylene on Nano Dendritic Copper Catalysts at High Current Density. *Adv. Energy Mater.* **2017**, 1602114.

(22) Grace, A. N.; Choi, S. Y.; Vinoba, M.; Bhagiyalakshmi, M.; Chu, D. H.; Yoon, Y.; Nam, S. C.; Jeong, S. K. Electrochemical reduction of carbon dioxide at low overpotential on a polyaniline/Cu_2O nanocomposite based electrode. *Appl. Energy* **2014**, *120*, 85–94.

(23) Ponnurangam, S.; Yun, C. M.; Chernyshova, I. V. Robust Electroreduction of CO_2 at a Poly(4-vinylpyridine)-Copper Electrode. *ChemElectroChem* **2015**, 74–82.

(24) Huang, Y.; Deng, Y.; Handoko, A. D.; Goh, G. K. L.; Yeo, B. S. Rational Design of Sulfur-Doped Copper Catalysts for the Selective Electroreduction of Carbon Dioxide to Formate. *ChemSusChem* **2017**, *138634*, 1–8.

(25) Huan, T. N.; Simon, P.; Benayad, A.; Guetaz, L.; Artero, V.; Fontecave, M. Cu/Cu_2O Electrodes and CO_2 Reduction to Formic Acid: Effects of Organic Additives on Surface Morphology and Activity. *Chem. Eur. J.* **2016**, 1–8.

(26) Aydin, R.; Dogan, H. Ö.; Köleli, F. Electrochemical reduction of carbon dioxide on polypyrrole coated copper electro-catalyst under ambient and high pressure in methanol. *Appl. Catal. B Environ.* **2013**, *140-141*, 478–482.

(27) Xie, M. S.; Xia, B. Y.; Li, Y.; Yan, Y.; Yang, Y.; Sun, Q.; Chan, S. H.; Fisher, A.; Wang, X. Amino acid modified copper electrodes for the enhanced selective electroreduction of carbon dioxide towards hydrocarbons. *Energy Environ. Sci.* **2016**, *9*, 1687–1695.

(28) Rochelle, G. T. Amine Scrubbing for CO_2 Capture. *Science* **2011**, *325*, 1652.

(29) Andreoli, E.; Dillon, E. P.; Cullum, L.; Alemany, L. B.; Barron, A. R. Cross-Linking Amine-Rich Compounds into High Performing Selective CO_2 Absorbents. *Sci. Rep.* **2014**, *4*, 1–5.

(30) Koutsianos, A.; Barron, A. R.; Andreoli, E. CO_2 capture partner molecules in highly loaded PEI sorbents. *J. Phys. Chem. C* **2017**, *121*, 21772–21781.

(31) Kresse, G.; Furthmüller, J. Efficient iterative schemes for ab initio total-energy calculations using a plane-wave basis set. *Phys. Rev. B* **1996**, *54*, 11169–11186.

(32) Perdew, J. P.; Burke, K.; Ernzerhof, M. Generalized Gradient Approximation Made Simple. *Phys. Rev. Lett.* **1996**, *77*, 3865–3868.

(33) Grimme, S.; Antony, J.; Ehrlich, S.; Krieg, H. A consistent and accurate ab initio parametrization of density functional dispersion correction (DFT-D) for the 94 elements H-Pu. *J. Chem. Phys.* **2010**, *132*.

(34) Henkelman, G.; Uberuaga, B. P.; Jónsson, H. Climbing image nudged elastic band method for finding saddle points and minimum energy paths. *J. Chem. Phys.* **2000**, *113*, 9901–9904.

(35) Tang, W.; Sanville, E.; Henkelman, G. A grid-based Bader analysis algorithm without lattice bias. *J. Phys. Condens. Matter* **2009**, *21*, 084204.

(36) Cheng, T.; Xiao, H.; Goddard, W. A. Full atomistic reaction mechanism with kinetics for CO reduction on Cu(100) from ab initio molecular dynamics free-energy calculations at 298 K. *Proc. Natl. Acad. Sci. U. S. A.* **2017**, *114*, 1795–1800.

(37) Shin, H. C.; Dong, J.; Liu, M. Nanoporous Structures Prepared by an Electrochemical Deposition Process. *Adv. Mater.* **2003**, *15*, 1610–1614.

(38) Nikolić, N. D.; Branković, G.; Pavlović, M. G.; Popov, K. I. The effect of hydrogen co-deposition on the morphology of copper electrodeposits. II. Correlation between the properties of electrolytic solutions and the quantity of evolved hydrogen. *J. Electroanal. Chem.* **2008**, *621*, 13–21.

(39) Nikolić, N. D.; Popov, K. I.; Pavlović, L. J.; Pavlović, M. G. Phenomenology of a formation of a honeycomb-like structure during copper electrodeposition. *J. Solid State Electrochem.* **2007**, *11*, 667–675.

(40) Nikolić, N. D.; Popov, K. I.; Pavlović, L. J.; Pavlović, M. G. The effect of hydrogen

codeposition on the morphology of copper electrodeposits. I. the concept of effective overpotential. *J. Electroanal. Chem.* **2006**, *588*, 88–98.

(41) Waszczuk, P.; Zelenay, P.; Sobkowski, J. Surface interaction of benzoic acid with a copper electrode. *Electrochim. Acta* **1995**, *40*, 1717–1721.

(42) Broekmann, P.; Fluegel, A.; Emnet, C.; Arnold, M.; Roeger-Goepfert, C.; Wagner, A.; Hai, N. T.; Mayer, D. Classification of suppressor additives based on synergistic and antagonistic ensemble effects. *Electrochim. Acta* **2011**, *56*, 4724–4734.

(43) Hai, N. T. M.; Kramer, K. W.; Fluegel, A.; Arnold, M.; Mayer, D.; Broekmann, P. Beyond interfacial anion/cation pairing: The role of Cu(I) coordination chemistry in additive-controlled copper plating. *Electrochim. Acta* **2012**, *83*, 367–375.

(44) Tan, K.; Tian, M. B.; Cai, Q. Effect of bromide ions and polyethylene glycol on morphological control of electrodeposited copper foam. *Thin Solid Films* **2010**, *518*, 5159–5163.

(45) Kelly, J. J.; Tian, C.; West, A. C. Leveling and Microstructural Effects of Additives for Copper Electrodeposition. *J. Electrochem. Soc.* **1999**, *146*, 2540–2545.

(46) Nam, D.; Kim, R.; Han, D.; Kim, J.; Kwon, H. Effects of $(NH_4)_2SO_4$ and BTA on the nanostructure of copper foam prepared by electrodeposition. *Electrochim. Acta* **2011**, *56*, 9397–9405.

(47) Gupta, N.; Gattrell, M.; MacDougall, B. Calculation for the cathode surface concentrations in the electrochemical reduction of CO_2 in $KHCO_3$ solutions. *J. Appl. Electrochem.* **2006**, *36*, 161–172.

(48) Texier, F.; Servant, L.; Bruneel, J. L.; Argoul, F. In situ probing of interfacial processes in the electrodeposition of copper by confocal Raman microspectroscopy. *J. Electroanal. Chem.* **1998**, *446*, 189–203.

(49) Moreno-Garcia, P.; Grimaudo, V.; Riedo, A.; Tulej, M.; Neuland, M. B.; Wurz, P.; Broekmann, P. Towards structural analysis of polymeric contaminants in electrodeposited Cu films. *Electrochim. Acta* **2016**, *199*, 394–402.

(50) Xu, F. Z.; Chen, S. G.; Chen, Y. Y.; Chen, Y. Corrosion resistance of 3,4-dihydroxyphenylalanine/octadecylamine complex coatings on copper substrate. *Mater. Corros.* **2013**, *64*, 69–73.

(51) Matos, J. B.; Pereira, L. P.; Agostinho, S. M.; Barcia, O. E.; Cordeiro, G. G.; D'Elia, E. Effect of cysteine on the anodic dissolution of copper in sulfuric acid medium. *J. Electroanal. Chem.* **2004**, *570*, 91–94.

(52) Kuhl, K. P.; Cave, E. R.; Abram, D. N.; Jaramillo, T. F. New Insights into the Electrochemical Reduction of Carbon Dioxide on Metallic Copper Surfaces. *Energy Environ. Sci.* **2012**, *5*, 7050–7059.

(53) Hori, Y.; Konishi, H.; Futamura, T.; Murata, A.; Koga, O.; Sakurai, H.; Oguma, K. "Deactivation of copper electrode" in electrochemical reduction of CO_2. *Electrochim. Acta* **2005**, *50*, 5354–5369.

(54) Levich, V. G. *Physicochemical hydrodynamics*; Englewood Cliffs, N. L., Prentice-Hall, 1962.

(55) Yang, K. D.; Ko, W. R.; Lee, J. H.; Kim, S. J.; Lee, H.; Lee, M. H.; Nam, K. T. Morphology-Directed Selective Production of Ethylene or Ethane from CO_2 on a Cu Mesopore Electrode. *Angew. Chem. Int. Ed.* **2016**, 796–800.

(56) Ren, D.; Deng, Y.; Handoko, A. D.; Chen, C. S.; Malkhandi, S.; Yeo, B. S. Selective Electrochemical Reduction of Carbon Dioxide to Ethylene and Ethanol on Copper(I) oxide catalysts. *ACS Catal.* **2015**, *5*, 2814–2821.

(57) Antonijevic, M. M.; Petrovic, M. B. Copper Corrosion Inhibitors. A review. *Int. J. Electrochem. Sci.* **2008**, *3*, 1–28.

(58) Mistry, H.; Varela, A. S.; Bonifacio, C. S.; Zegkinoglou, I.; Sinev, I.; Choi, Y.-w.; Kisslinger, K.; Stach, E. A.; Yang, J. C.; Strasser, P.; Cuenya, B. R. Highly selective plasma-activated copper catalysts for carbon dioxide reduction to ethylene. *Nat. Commun.* **2016**, *7*, 1–8.

(59) Eilert, A.; Cavalca, F.; Roberts, F. S.; Osterwalder, J.; Liu, C.; Favaro, M.; Crumlin, E. J.; Ogasawara, H.; Friebel, D.; Pettersson, L. G.; Nilsson, A. Subsurface Oxygen in Oxide-Derived Copper Electrocatalysts for Carbon Dioxide Reduction. *J. Phys. Chem. Lett.* **2017**, *8*.

(60) Xiao, H.; Goddard, W. A.; Cheng, T.; Liu, Y. Cu metal embedded in oxidized matrix catalyst to promote CO_2 activation and CO dimerization for electrochemical reduction of CO_2. *Proc. Natl. Acad. Sci. U. S. A.* **2017**, 201702405.

(61) Vaduva, C. C.; Vaszilcsin, N.; Kellenberger, A. Aromatic amines as proton carriers for catalytic enhancement of hydrogen evolution reaction on copper in acid solutions. *Int. J. Hydrog. Energy* **2012**, *37*, 12089–12096.

(62) Vaduva, C. C.; Vaszilcsin, N.; Kellenberger, A.; Medeleanu, M. Catalytic enhancement of hydrogen evolution reaction on copper in the presence of benzylamine. *Int. J. Hydrog. Energy* **2011**, *36*, 6994–7001.

(63) Luo, W.; Nie, X.; Janik, M. J.; Asthagiri, A. Facet Dependence of CO_2 Reduction Paths on Cu Electrodes. *ACS Catal.* **2016**, *6*, 219–229.

(64) Sandberg, R. B.; Montoya, J. H.; Chan, K.; Nørskov, J. K. CO-CO coupling on Cu facets: Coverage, strain and field effects. *Surf. Sci.* **2016**, *654*, 56–62.

(65) Perez-Gallent, E.; Figueiredo, M. C.; Calle-Vallejo, F.; Koper, M. T. M. Spectroscopic Observation of a Hydrogenated CO Dimer Intermediate During CO Reduction on Cu(100) Electrodes. *Angew. Chem. Int. Ed.* **2017**, *56*, 3621–3624.

(66) Montoya, J. H.; Shi, C.; Chan, K.; Nørskov, J. K. Theoretical Insights into a CO Dimerization Mechanism in CO_2 Electroreduction. *J. Phys. Chem. Lett.* **2015**, *6*, 2032–2037.

(67) Yano, H.; Tanaka, T.; Nakayama, M.; Ogura, K. Selective electrochemical reduction of CO_2 to ethylene at a three-phase interface on copper(I) halide-confined Cu-mesh electrodes in acidic solutions of potassium halides. *J. Electroanal. Chem.* **2004**, *565*, 287–293.

(68) Ogura, K.; Oohara, R.; Kudo, Y. Reduction of CO_2 to Ethylene at Three-Phase Interface Effects of Electrode Substrate and Catalytic Coating. *J. Electrochem. Soc.* **2005**, *152*, D213.

(69) Huang, Y.; Handoko, A. D.; Hirunsit, P.; Yeo, B. S. Electrochemical Reduction of CO_2 Using Copper Single-Crystal Surfaces: Effects of CO* Coverage on the Selective Formation of Ethylene. *ACS Catal.* **2017**, *7*, 1749–1756.

Graphical TOC Entry

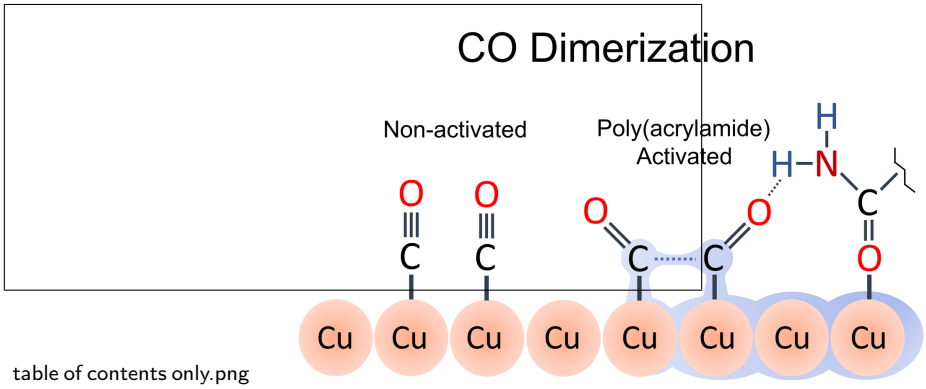

table of contents only.png

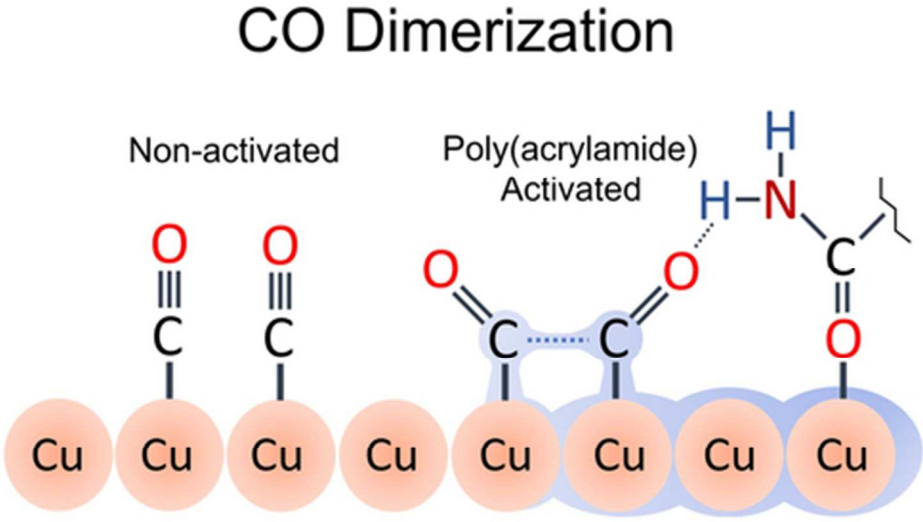

TOC

44x23mm (300 x 300 DPI)